



HAL
open science

Pou3f transcription factor expression during embryonic development highlights distinct pou3f3 and pou3f4 localization in the *Xenopus laevis* kidney

Camille Cosse-Etchepare, Isabelle Gervi, Isabelle Buisson, Laurent Formery, Michael Schubert, Jean-François Riou, Muriel Umbhauer, Ronan R. Le Bouffant

► To cite this version:

Camille Cosse-Etchepare, Isabelle Gervi, Isabelle Buisson, Laurent Formery, Michael Schubert, et al.. Pou3f transcription factor expression during embryonic development highlights distinct pou3f3 and pou3f4 localization in the *Xenopus laevis* kidney. *International Journal of Developmental Biology*, 2018, 62 (4-5), pp.325-333. 10.1387/ijdb.170260RL . hal-02117425

HAL Id: hal-02117425

<https://hal.science/hal-02117425v1>

Submitted on 29 Oct 2021

HAL is a multi-disciplinary open access archive for the deposit and dissemination of scientific research documents, whether they are published or not. The documents may come from teaching and research institutions in France or abroad, or from public or private research centers.

L'archive ouverte pluridisciplinaire **HAL**, est destinée au dépôt et à la diffusion de documents scientifiques de niveau recherche, publiés ou non, émanant des établissements d'enseignement et de recherche français ou étrangers, des laboratoires publics ou privés.

***Pou3f* transcription factor expression during embryonic development highlights distinct *pou3f3* and *pou3f4* localization in the *Xenopus laevis* kidney**

CAMILLE COSSE-ETCHEPARE¹, ISABELLE GERVI¹, ISABELLE BUISSON¹, LAURENT FORMERY²,
MICHAEL SCHUBERT², JEAN-FRANÇOIS RIOU¹, MURIEL UMBHAUER^{*,1} and RONAN LE BOUFFANT^{*,1}

¹Sorbonne Université, CNRS Biologie du Développement, Institut de Biologie Paris-Seine (IBPS), Paris and

²Sorbonne Université, CNRS, Laboratoire de Biologie du Développement de Villefranche-sur-Mer, Observatoire Océanologique de Villefranche-sur-Mer, Villefranche-sur-Mer, France


ABSTRACT The *POU* (*Pit-Oct-Unc*) genes encode a large transcription factor family comprising 6 classes (*pou1f* to *pou6f*) involved in many developmental processes, such as cell commitment and differentiation. The *pou3f* class contains four members (*pou3f1*, *pou3f2*, *pou3f3*, *pou3f4*) characterized by expression in ectodermal tissue derivatives, such as nervous system and otic vesicle, during mammalian development. In order to obtain insights into the potential conservation of this class of transcription factors in vertebrates, we carried out a phylogenetic analysis and a comprehensive comparative study of *pou3f* expression in the frog *Xenopus laevis*. All vertebrates examined possessed members of the four *pou3f* subfamilies, excepting the zebrafish, which lacked a *pou3f4* gene. Whole mount *in situ* hybridization and real-time quantitative polymerase chain reaction (RT-qPCR) analyses revealed that *Xenopus pou3f* genes were expressed in the forming neural tube and their expression was maintained in the brain, mostly in the dorsal part, at tailbud stages. The *pou3f2*, *pou3f3*, and *pou3f4* genes were also expressed in the developing otic vesicle, and *pou3f1* in some cells of the epidermis. Besides ectodermal derivatives, *pou3f3* and *pou3f4* were expressed in the developing kidney. Their expression started at the early tailbud stage in the pronephric anlage and partly overlapped. In the mature pronephric tubule, *pou3f3* was restricted to the intermediate tubule, while *pou3f4* was also expressed in the distal and connecting tubule. Together, our results highlight a significant conservation of *pou3f* gene expression in vertebrates and indicate that they may have distinct but also redundant functions during neural and renal development.

KEY WORDS: *Pou3f*, embryo, kidney, *Xenopus laevis*

Transcription factors serve critical roles in cell commitment and subsequent differentiation during organ formation. The *POU* (*Pit-Oct-Unc*) genes encode a large family of transcription factors known for their roles during development (Ryan and Rosenfeld, 1997). They are defined by the presence of a highly conserved bipartite DNA-binding domain, the POU-domain, consisting of an approximately 75 amino acid N-terminal POU-specific domain and a 60 amino acid C-terminal POU-homeodomain. These two subdomains are tethered by a linker of variable length (14-26 amino acids) (Ryan and Rosenfeld, 1997). The acronym POU is derived from

the names of the first genes in which the POU-domain has been discovered, i.e. the three mammalian transcription factors *Pit-1*, *Oct-1/2*, and the *Caenorhabditis elegans* developmental regulator *unc86*. The POU-domain proteins have since been described in a wide variety of animal species, but have not yet been identified in fungi or plants. In mammals, they have been grouped into six classes (*Pou1f* to *Pou6f*), depending on the amino acid sequence of their

Abbreviations used in this paper: POU, Pit-Oct-Unc; RT-qPCR, real-time quantitative polymerase chain reaction.

*Address correspondence to: Muriel Umbhauer -  <https://orcid.org/0000-0001-7419-8070> and Ronan Le Bouffant -  <https://orcid.org/0000-0002-0995-7373>
Sorbonne Université, CNRS-Biologie du Développement, Institut de Biologie Paris-Seine (IBPS), 9 quai Saint-Bernard, 75005 Paris, France. Tel: +33 1 44 27 29 01.
E-mails: ronan.le_bouffant@upmc.fr - muriel.umbhauer@upmc.fr

Supplementary Material (3 figures + 3 tables) for this paper is available at: <http://dx.doi.org/10.1387/ijdb.170260RL>

Submitted: 17 October, 2017; Accepted: 9 November, 2017.

POU-domain and the conservation of the variable linker region.

The Pou3f class is composed of 4 intronless genes, *pou3f1* (alternatively called *oct6*, *otf6*, *pou50*, *scip*, *test1*, *tst1*, *nrl-22* or *XLPOU1*), *pou3f2* (alternatively called *BRN2*, *OCT7*, *OTF7*, *OTF-7*, *POUF3*, *brn-2*, *oct-7* or *N-Oct3*), *pou3f3* (alternatively called *BRN1*, *OTF8*, *oct-8* or *brain-1*), and *pou3f4* (alternatively called *BRAIN-4*, *BRN-4*, *BRN-4*, *DFN3*, *DFNX2*, *OCT-9*, *OTF-9* or *OTF9*). They have been shown to be involved in neural and ectodermal development in mammals. Pou3f1 promotes neural fate commitment during mouse gastrulation (Zhu et al., 2014). It is implicated in Schwann cell myelination and oligodendrocyte as well as keratinocyte differentiation (Zhao, 2013). Pou3f2 is a regulator of melanocyte growth and tumorigenesis. It is responsive to MAPK pathway activation and modulates the levels of the transcription factor MITF, hence preventing melanocytic differentiation ultimately leading to tumor metastasis (Cook and Sturm, 2008). Pou3f4 is implicated in neuron and otic vesicle development, where it controls cochlea formation. In humans, defects in POU3F4 cause X-linked deafness type 3 (Zhao, 2013). Pou3f transcription factors can act redundantly during embryonic development. In single *Pou3f2* or *Pou3f3* mouse mutants, no developmental defects are observable in the neocortex where these genes are co-expressed, while the double mutants of both *Pou3f2* and *Pou3f3* are characterized by abnormal formation of the neocortex with dramatically reduced production of layer II-IV neurons and defective migration of neurons (Cook and Sturm, 2008).

The expression of *pou3f* genes is documented principally in the vertebrate nervous system, but data appear fragmented. An exhaustive spatial and temporal expression survey for all *pou3f* genes is clearly missing in the literature. We therefore performed this analysis using the frog *Xenopus laevis* as a model and first assessed the conservation, phylogeny, and synteny of vertebrate *pou3f* class genes. We then described the expression patterns of each *pou3f* gene during *X. laevis* embryonic development. Our results highlight a high level of conservation of *pou3f* class genes across vertebrates. In *X. laevis*, partially overlapping expression in the developing neural tube suggests a potentially conserved function during vertebrate brain development. We also find that *pou3f3* and *pou3f4* genes are partially co-expressed in the developing pronephros, a first in any vertebrate.

Results

Evolutionary conservation of Pou3f class members

In order to characterize the evolution of Pou3f class members in vertebrates, we first analyzed alignments of the amino acid sequences of selected Pou3f proteins (Figs. 1; S1). In *X. laevis*, each *Pou3f* gene has two homologous copies (L and S), whose mRNA coding sequences and protein sequences are highly conserved (more than 99% of identity). We therefore performed the alignments with only one homolog. Alignment of the four *X. laevis* Pou3f proteins (Pou3f1, Pou3f2, Pou3f3, Pou3f4) revealed a particularly high degree of sequence conservation in the POU-specific

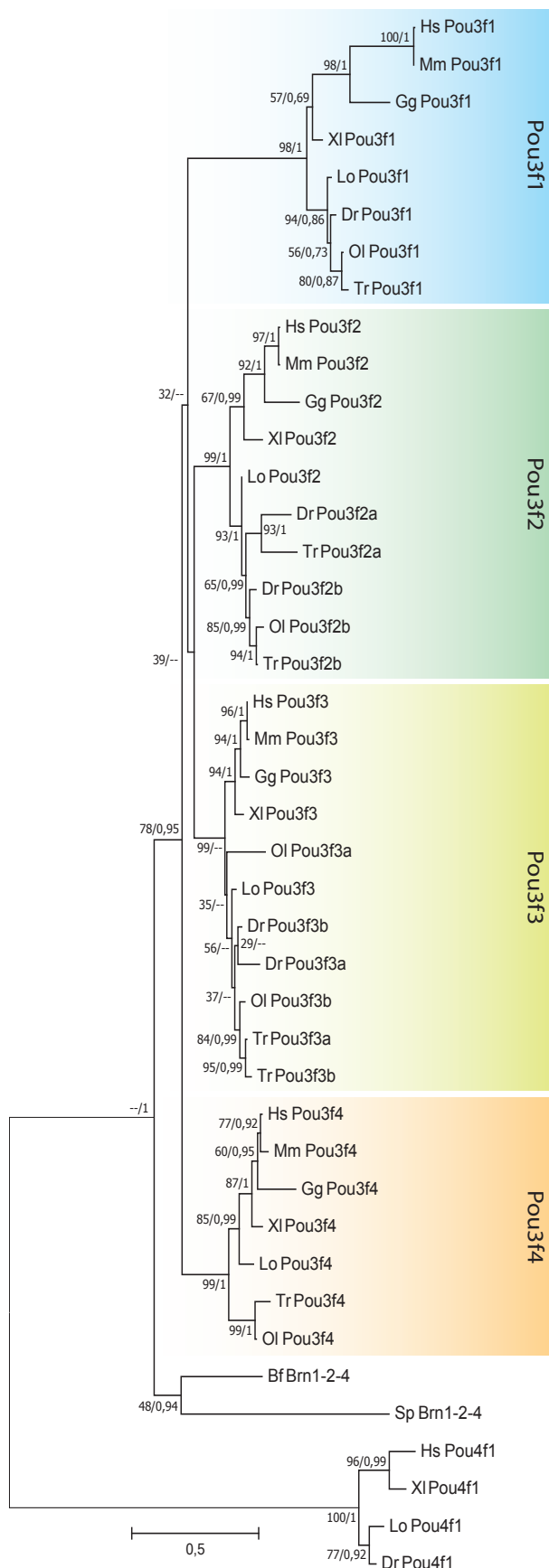
A

Xl_Pou3f1	--MAATAQYL	PRNNSLPSNP	LMHPDSDRMH	QGT-----	---YR--EVQ	KMMHQEYLQG	L--ATNAGHP	MSLTHHQWLP	NPTSDWGS	HLGAQAEHGK	SGVQS-----	-----SRE
Xl_Pou3f2	--MATTASN-	HYNLLGSGSS	IVHADPGGMQ	QAQS-----	---YR--DAQ	TLVQSDYT--	L--QSN-GHP	LSHAHQWITA	LSHGDGAPWA	TSPLGQQDIK	PTVQS-----	-----SRD
Xl_Pou3f3	MATAASNPLY	PSNSILSPGS	IVHSDSGGGM	QPGSAAVTSV	AGGYRGDPTV	KMVQSDFMQ	AMAASNGGHH	LSHAHQWVTA	LPHAAAAAAA	AAAAAAEAGS	HWSSSPVGMT	GSPQHPQQQQ
Xl_Pou3f4	MATAASNPY-	---SILSSSS	LVHADSAVMQ	QGSP-----	---FR--NPQ	KLLQSDYLQG	V---PCNGHP	LG--HHWVTS	L--SDANPWS	SSLASSPLDQ	QDIKP-----	-----GRE
Xl_Pou3f1	DLSSSF---H	HHRSLHLVHQ	Q---TPSSH-	--AWAQSGGH	HLPSPSPGS-	-----N	SHQPLIYSQS	SYTNLNGMLG	PQASS--LHH	-----SMRDP	LHDDPGVHDT	HVESPPQHL-
Xl_Pou3f2	ELHVSGLTQH	QSRAPHLVHP	A---HGNHHG	PGAWRSTGST	HLSSMA--S-	-----S	NGQGLIYSQP	SFT-VNGMIN	PGSGQGIHHH	-----GLRDS	HDDHGDHGH	QVVSQAQQQH
Xl_Pou3f3	DVKGGAGRDE	LHPGAAALHR	PHLAPHQGH	PGWGAAAAAS	HIQSMAGATP	QQQQQQQQQQ	QQQALLYSQP	GAFTVNGMLS	PPPGSQNLVH	PGLVRGDTPE	LGDHPGHHH	HHHQHQHHQ
Xl_Pou3f4	DLQLGAI--	HHRSPVNH	---SPHTNH	PNAWGASPAH	NSSLTS----	-----S	GQPINIYSQP	SFT-VSGMLD	HGELTPPLPA	-----GTTQS	LHPVLRPNP	HVDLGSHHHC-
Xl_Pou3f1	---GHH---	---QDHSDED	APSSDDLEQF	AKQFKQRRIK	LGFTQADVGL	ALGTLYGNVF	SQTTICRFEA	LQLSFKNMCK	LKPLLNKWLE	ETDSTGTSPT	NLDKIAAQR	KRKRKTSIEV
Xl_Pou3f2	SQQLGGH---	---QDHSDED	TPTSDDLEQF	AKQFKQRRIK	LGFTQADVGL	ALGTLYGNVF	SQTTICRFEA	LQLSFKNMCK	LKPLLNKWLE	EADSSSGSPT	SIDKIAAQR	KRKRKTSIEV
Xl_Pou3f3	QQQQHHGGV	NSHDPHSDED	TPTSDDLEQF	AKQFKQRRIK	LGFTQADVGL	ALGTLYGNVF	SQTTICRFEA	LQLSFKNMCK	LKPLLNKWLE	EADSTGTSPT	SIDKIAAQR	KRKRKTSIEV
Xl_Pou3f4	-----	---QDHSDEE	TPTSDDLEQF	AKQFKQRRIK	LGFTQADVGL	ALGTLYGNVF	SQTTICRFEA	LQLSFKNMCK	LKPLLNKWLE	EADSTGNPT	SIDKIAAQR	KRKRKTSIEV
Xl_Pou3f1	GVKGALENHF	LKCKPSPAHE	ITSLADSLQL	EKEVVRVWFC	NRRQKEKRM	PAGVPHPE	DVYSQ----	AETPLHHTL	QTSVQ			
Xl_Pou3f2	SVKGALESHF	LKCKPSPAHE	ITSLADSLQL	EKEVVRVWCC	NRRQKEKRM	PFGGTIPGAE	DIYGA----	SRDTPHLGV	QTSVQ			
Xl_Pou3f3	SVKGALESHF	LKCKPSPAHE	ITSLADSLQL	EKEVVRVWFC	NRRQKEKRM	PFGIQQQTPD	DVYSQVGNVG	ADTPPHHGM	QTSVQ			
Xl_Pou3f4	SVKGVLETHF	LKCKPSPAHE	ITSLADSLQL	EKEVVRVWFC	NRRQKEKRM	PFGDPQ--H	EVYSHSVKTD	TSCNEL----				

B

	POU-specific domain	Linker	Homeodomain	Full-length protein
Pou3f1	100%	91%	96%	68%
Pou3f2	100%	95%	96%	72%
Pou3f3	100%	98%	98%	75%
Pou3f4	100%	92%	96%	85%

Fig. 1. Sequence analysis of vertebrate Pou3f proteins. (A) Sequence alignments of the *Xenopus laevis* (Xl) *Pou3f1*, *Pou3f2*, *Pou3f3*, and *Pou3f4* proteins. Conserved residues are shown in bold, the POU-specific domain and the POU-homeodomain are highlighted in yellow, and the linker region is indicated in cyan. (B) The percentage of sequence identity for each vertebrate *Pou3f* subfamily (*Pou3f1*, *Pou3f2*, *Pou3f3*, and *Pou3f4*) relative to the *Xenopus laevis* sequence is indicated for the POU-specific domain, the linker, the POU-homeodomain as well as for the whole (i.e. full-length) protein. The percentages are the average sequence identities of the human (*Homo sapiens*), mouse (*Mus musculus*), chicken (*Gallus gallus*), and spotted gar (*Lepisosteus oculatus*) sequences relative to the African clawed frog (*Xenopus laevis*) sequence.



domain, the linker region as well as the POU-homeodomain (Fig. 1A). Comparisons of the four *X. laevis* Pou3f class proteins with their respective orthologs from human, mouse, chicken, and the spotted gar further supported this finding, with sequence identities ranging between 68% and 85% for the full-length proteins, but reaching 100% within the POU-specific domain, between 91% and 98% in the linker region, and between 96% and 98% in the POU-homeodomain (Fig. 1B). To assess the evolutionary diversification of *pou3f* class genes in vertebrates, we next performed phylogenetic analyses of Pou3f proteins (Figs. 2, S1). The resulting phylogenetic tree revealed that the vertebrate *pou3f* genes encoding these proteins group into four subfamilies (*pou3f1*, *pou3f2*, *pou3f3*, *pou3f4*), with each vertebrate analyzed possessing at least one member of each of these subfamilies (Fig. 2), except for the zebrafish that lacks a *pou3f4* gene. The phylogeny further revealed that the genomes of teleost fish encode additional paralogs in the *pou3f2* and *pou3f3* subfamilies and that some fish lineages might have independently lost specific *pou3f* genes, which seems to be the case for zebrafish *pou3f4* as well as for medaka *pou3f2a* (Fig. 2). Of note, non-vertebrates seem to generally possess only a single *pou3f* gene (Fig. 2). To further investigate the evolution of *pou3f* genes in vertebrates, we next carried out a synteny analysis of the *pou3f* loci of several vertebrate species (Fig. 3). This analysis largely supported the results obtained by the phylogenetic tree reconstruction in that, while vertebrate genomes are generally characterized by at least four *pou3f* genes, the genomes of teleost fish have experienced both additional large-scale duplications (resulting in additional teleost *pou3f2* and *pou3f3* paralogs) and species-specific *pou3f* gene losses (leading to the absence of zebrafish *pou3f4* and medaka *pou3f2a*) (Fig. 3).

Spatial and temporal expression of *pou3f1* during *X. laevis* development

Temporal and spatial expression of *pou3f1* during *X. laevis* embryonic development was examined by real-time quantitative polymerase chain reaction (RT-qPCR) and whole mount *in situ* hybridization. *Pou3f1* expression begins at gastrulation (st 10), increases during neurulation (st 13-16) and tailbud stages (st 22) to reach a maximum level at the late tailbud stage (st 28), with its expression subsequently decreasing at the tadpole stage (st 37) (Fig. 4A). By *in situ* hybridization, the signal is first detected in the marginal zone during gastrulation (Fig. 4B, a). At the mid-neurula

Fig. 2. Phylogenetic relationship of vertebrate Pou3f proteins. Phylogenetic tree of the Pou3f family based on sequences from human (*Homo sapiens*, Hs), mouse (*Mus musculus*, Mm), chicken (*Gallus gallus*, Gg), African clawed frog (*Xenopus laevis*, XI), zebrafish (*Danio rerio*, Dr), medaka (*Oryzias latipes*, Ol), Japanese puffer (*Takifugu rubripes*, Tr), spotted gar (*Lepisosteus oculatus*, Lo), Florida amphioxus (*Branchiostoma floridae*, Bf), and the purple sea urchin (*Strongylocentrotus purpuratus*, Sp). The Pou3f1, Pou3f2, Pou3f3, and Pou3f4 subfamilies are respectively highlighted in blue, green, yellow, and orange. The tree was rooted with members of the Pou4f1 subfamily. Although trees were calculated using both the Maximum Likelihood (ML) and Bayesian Inference (BI) methods, only the ML tree is shown, with branch lengths being representative of sequence substitution rates. Branch support is indicated as bootstrap percentages from the ML analysis (ranging from 0 to 100) / posterior probabilities (ranging from 0 to 1) from the BI analysis. "--" indicates that the branching patterns of the ML and BI analyses diverged at this node and that one of the scores is thus unavailable.

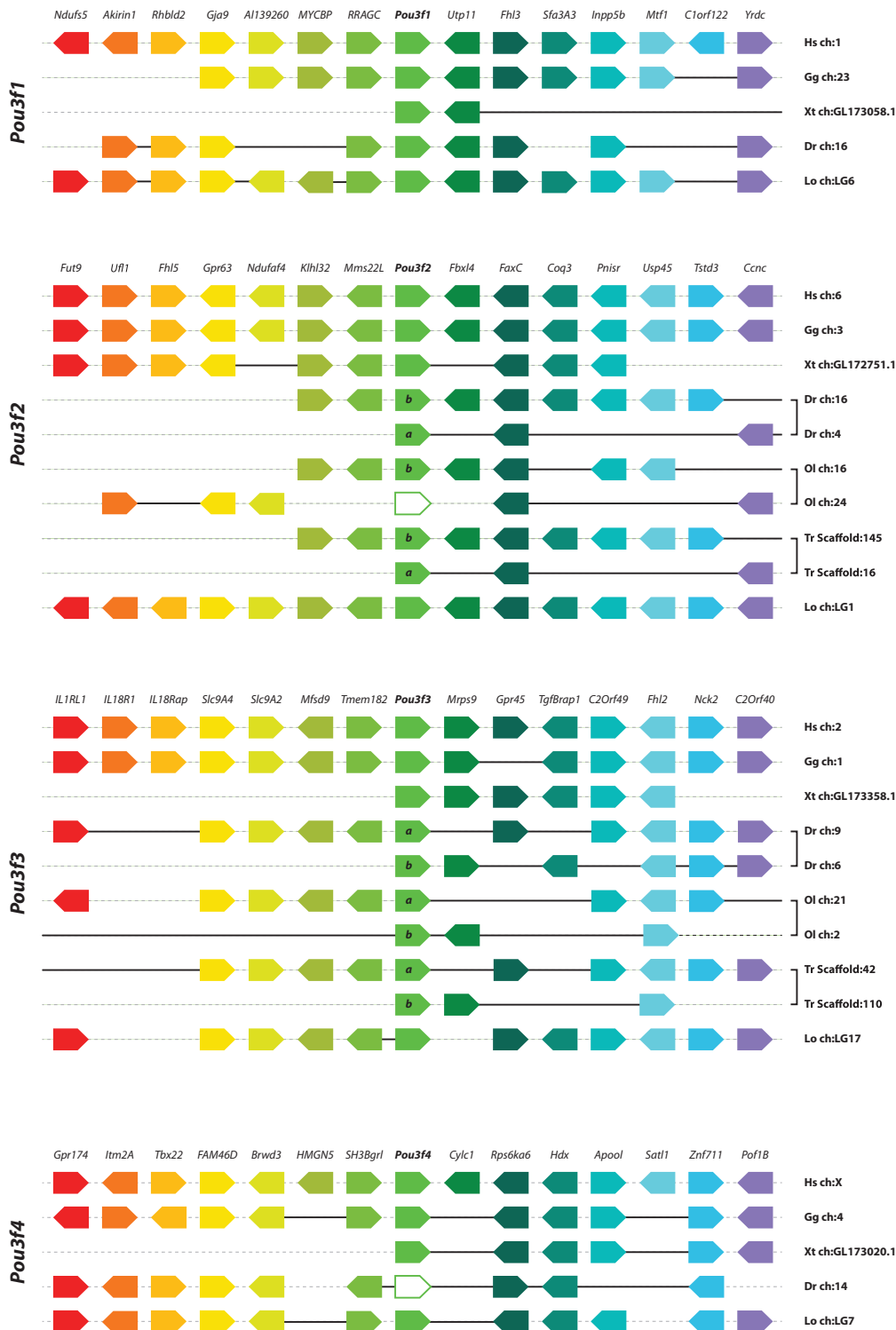


Fig. 3. Genomic organization of vertebrate *pou3f* loci. Genomic organization and gene synteny comparisons of vertebrate *pou3f1*, *pou3f2*, *pou3f3*, and *pou3f4* genes. Dotted lines represent chromosome loci in the genomes of human (*Homo sapiens*, Hs), chicken (*Gallus gallus*, Gg), Western clawed frogs (*Xenopus tropicalis*, Xt), zebrafish (*Danio rerio*, Dr), medaka (*Oryzias latipes*, Ol), Japanese puffers (*Takifugu rubripes*, Tr), and spotted gars (*Lepisosteus oculatus*, Lo). Genes are shown as colored pentagon arrows, with the transcriptional orientation of a given gene locus being indicated by the direction of the arrow. When a *pou3f* paralog is not found in a given species, the pentagon is white. Gene loci are named according to the nomenclature used in human and orthologs in the different species are shown in identical colors. Gene paralogs are indicated by letters. Bold black lines between polygons mark changes in genetic linkage and hence in gene synteny relative to the situation in the human genome.

stage (st 16), *pou3f1* is expressed in the anterior neural folds (Fig. 4B, c), and its expression is maintained in the lateral part of the neural tube all along its antero-posterior axis at stage 23 (Fig. 4B, d, e). Subsequently, *pou3f1* is expressed in the dorsal half of the brain excepting the most dorsal part at late tailbud and tadpole stages (Fig. 4B, f-i). Transcripts of *pou3f1* are also found in the optic vesicle at the early tailbud stage (Fig. 4B, d) and in the retina at later stages (Fig. 4B, f-i). In addition, from the early tailbud stage onward, there is a strong dotted staining of *pou3f1* in the epidermis, and, from the mid-neurula stage, *pou3f1* expression is further detectable in neuro-ectodermal tissues. This spatial expression pattern was confirmed by RT-qPCR analysis of different embryonic regions: these results clearly showed a relative enrichment of *pou3f1* transcripts in the dorsal half of the embryo as well as in the head (Fig. 4C).

Spatial and temporal expression of *pou3f2* during *X. laevis* development

RT-qPCR analysis revealed a high variability of *pou3f2* expression levels, likely due to the very dynamic expression pattern of *pou3f2* (data not shown). Expression is not detectable by whole mount *in situ* hybridization before the early neurula stage when it is detectable in the anterior part of the neural plate as a stripe in the neural folds (Fig. 5A, a,b). Its neural expression is restricted to the brain during tailbud and tadpole stages (Fig. 5A, c-i). Examination of transverse sections at the early tailbud stage (st 23) highlights expression in the dorso-lateral part of the hindbrain (Fig. 5A, d). The *pou3f2* gene is also expressed in the otic vesicle at late tailbud stages (st 29/30-39) (Fig. 5A, e,f,h,i) and in two cell populations ventral to the eye that might be neural crest cell derivatives (arrowhead) (Fig. 5A, f,i). This spatial expression pattern was confirmed by RT-qPCR analysis of different embryonic regions, showing a strong relative enrichment of *pou3f2* transcripts in the head (Fig. 5B).

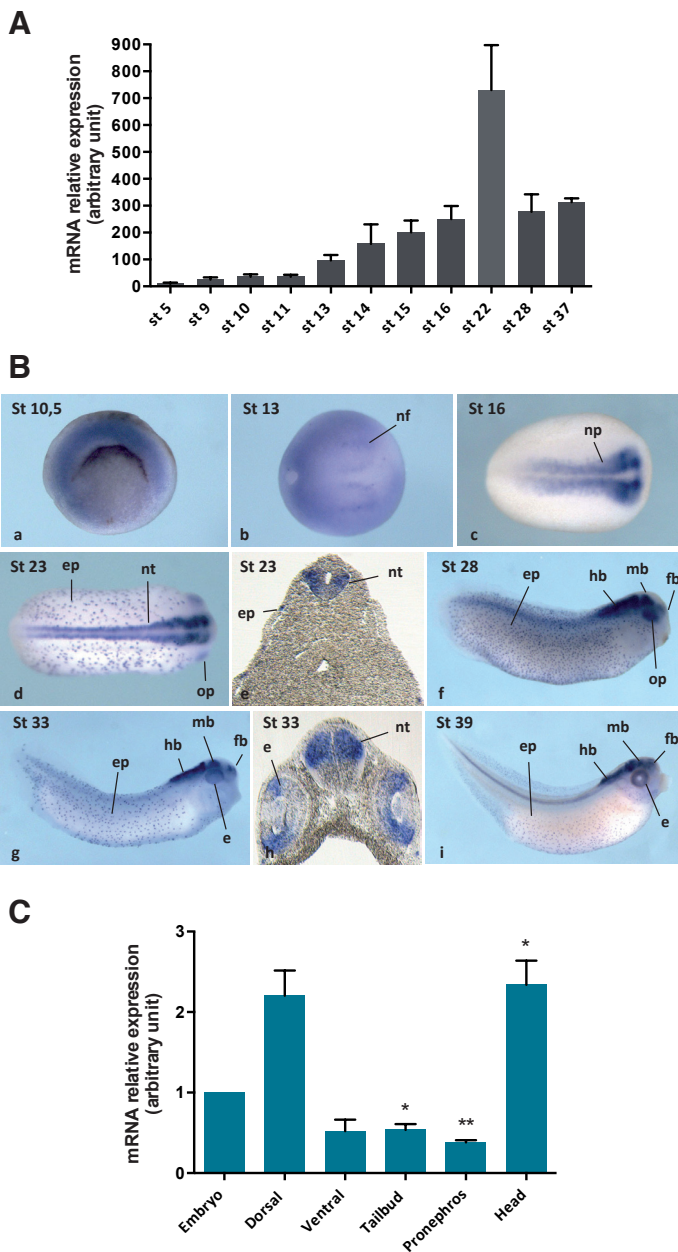


Fig. 4 (left). Spatio-temporal expression of *pou3f1* during *Xenopus laevis* development. (A) Expression of *pou3f1* analyzed by real-time quantitative polymerase chain reaction (RT-qPCR) at indicated stages of development. Average values from three independent experiments. (B) Whole mount in situ hybridization for *pou3f1* at indicated stages of development. Early gastrula, vegetal view (a). Neurula, dorsal view (b,c). Tailbud, dorsal (d) and lateral (f) view. Tadpole, lateral view (g,i). Transverse sections at the level of the developing brain at tailbud stage (e) and at the level of the developing eye at tadpole stage (h). Abbreviations: e, eye; ep, epidermis; fb, forebrain; hb, hindbrain; mb, midbrain; nf, neural fold; np, neural plate; nt, neural tube; op, optic placode. (C) Expression of *pou3f1* analyzed by RT-qPCR on dissected explants from tailbud-stage embryos, stage 25. Embryos were dissected either into ventral and dorsal halves or into tailbud, pronephros and head. Average values from three independent experiments. *: $P < 0,05$; **: $P < 0,005$, relative to the whole embryo.

Spatio and temporal expression of *pou3f3* during *X. laevis* development

RT-qPCR detected no maternal *pou3f3* expression and very low levels of expression during gastrulation. *Pou3f3* expression increases slowly during neurulation (st 13-16) and during tailbud stages (st 22 and 28), before decreasing at the tadpole stage (st 37) (Fig 6A). *Pou3f3* transcripts were first detected by *in situ* hybridization in the anterior neural plate as a stripe in the neural folds (Fig. 6B, a,b). From the early tailbud stage, *pou3f3* is strongly

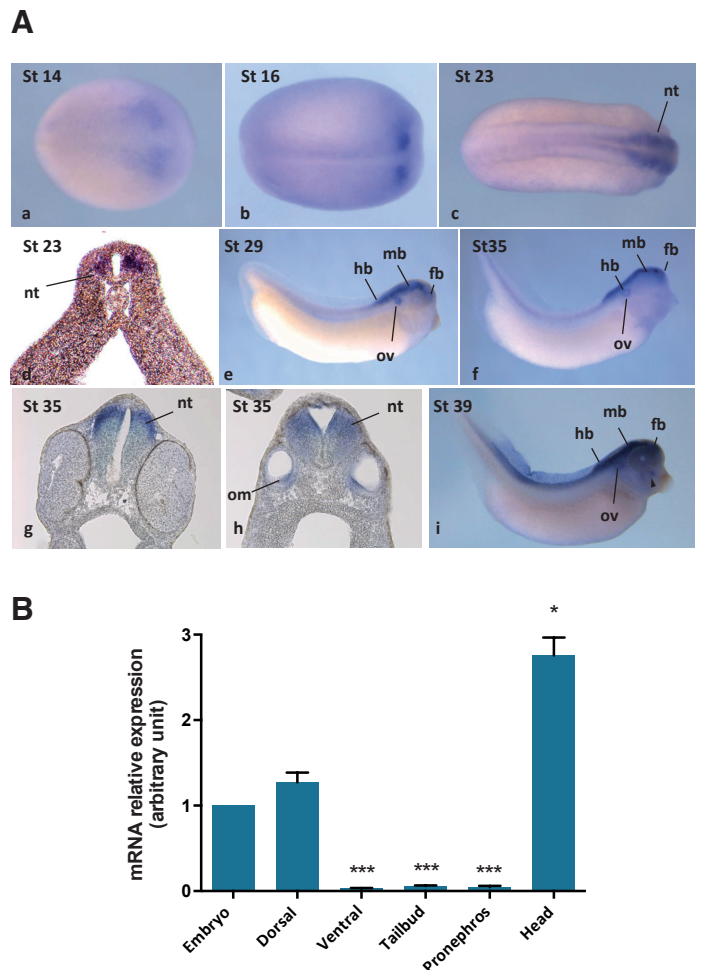


Fig. 5 (right). Spatio-temporal expression of *pou3f2* during *Xenopus laevis* development. (A) Whole mount in situ hybridization for *pou3f2* at indicated stages of development. Neurula, dorsal view (a,b). Tailbud, dorsal (c) and lateral (e) view. Tadpole, lateral view (f,i). Transverse sections at the level of the developing brain (d,g,h), and otic vesicle (h). Abbreviations: (fb) forebrain, (hb) hindbrain, (mb) midbrain, (nt) neural tube, (om) otic mesenchyme, (ov) otic vesicle. (B) Expression of *pou3f2* analyzed by real-time quantitative polymerase chain reaction (RT-qPCR) on dissected explants from tailbud embryos (stage 25). Embryos were dissected either into ventral and dorsal halves or into tailbud, pronephros and head. *: $P < 0,05$; ***: $P < 0,001$, relative to the whole embryo.

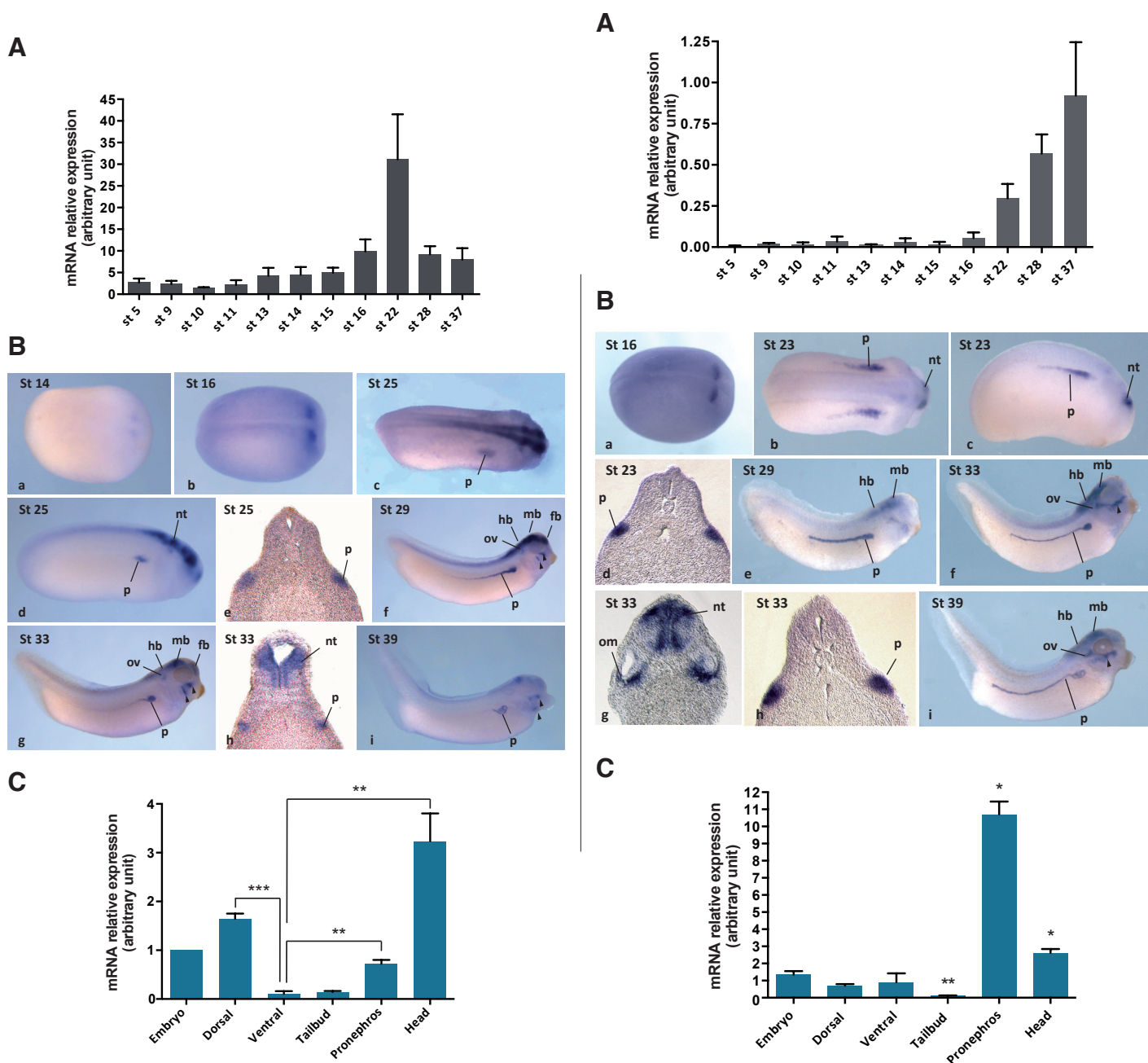


Fig. 6 (left). Spatio-temporal expression of *pou3f3* during *Xenopus laevis* development. (A) Expression of *pou3f3* analyzed by real-time quantitative polymerase chain reaction (RT-qPCR) at indicated stages of development. **(B)** Whole mount in situ hybridization for *pou3f3* at indicated stages of development. Neurula, dorsal view (a,b). Tailbud, dorsal (c) and lateral (d,f) view. Tadpole, lateral view (g,i). Transverse sections at the level of the developing pronephros (e,h). Abbreviations: (fb) forebrain, (hb) hindbrain, (mb) midbrain, (nt) neural tube, (ov) otic vesicle, (p) pronephros. **(C)** Expression of *pou3f3* analyzed by RT-qPCR on dissected explants from tailbud-stage embryos (stage 25). Embryos were dissected either into ventral and dorsal halves or into tail bud, pronephros and head. **: $P < 0,005$; ***: $P < 0,001$, relative to the ventral half.

Fig. 7 (right). Spatio-temporal expression of *pou3f4* during *Xenopus laevis* development. (A) Expression of *pou3f4* analyzed by real-time quantitative polymerase chain reaction (RT-qPCR) at indicated stages of development. Average values from three independent experiments. **(B)** Whole mount in situ hybridization for *pou3f4* at indicated stages of development. Neurula, dorsal view (a). Tailbud, dorsal (b) and lateral view (c,e). Tadpole, lateral (f,i) view. Transverse sections at the level of the developing pronephros (d,h) and otic vesicle (g). Abbreviations: (fb) forebrain, (hb) hindbrain, (mb) midbrain, (nt) neural tube, (om) otic mesenchyme, (ov) otic vesicle, (p) pronephros. **(C)** Expression of *pou3f4* analyzed by RT-qPCR on dissected explants from tailbud-stage embryos (stage 25). Embryos were dissected either into ventral and dorsal halves or into tail bud, pronephros and head. *: $P < 0,05$; **: $P < 0,005$, relative to the whole embryo.

expressed in the developing forebrain, midbrain, and hindbrain where expression is maintained at least until the tadpole stage (Fig. 6B, c-i). Outside the brain, *pou3f3* is also detectable in the developing pronephros. At the early tailbud stage, transcripts are present in the proximal part of the pronephric anlage (Fig. 6B, d,e). Pronephric expression of *pou3f3* persists in the developing tubule during tailbud and tadpole stages (Fig. 6B, f-i). *Pou3f3* is also expressed in the otic vesicle and possibly in anterior neural crest cell derivatives (arrowhead) (Fig. 6B, f,g,i). RT-qPCR analysis of different regions of early tailbud stage embryos confirmed these observations, with strong relative expression of *pou3f3* in the head and pronephros (Fig. 6C, S2).

Spatial and temporal expression of *pou3f4* during *X. laevis* development

Pou3f4 starts to be weakly expressed in the embryo at the mid-neurula stage (st 16), and its expression gradually increases during tailbud (st 22 and 28) and tadpole stages (st 37), as shown by RT-qPCR (Fig. 7A). Using whole mount *in situ* hybridization, *pou3f4* transcripts were first detectable at the mid-neurula stage in the anterior part of the neural folds (Fig. 7B, a). At tailbud stages, *pou3f4* expression is conspicuous in the developing midbrain and hindbrain where it is maintained at tadpole stages (Fig. 7B, e,f,g,i). Apart from the brain, *pou3f4* is also strongly expressed in the pronephric anlage at the early tailbud stage (Fig. 7B, b-d), with expression persisting in the developing pronephric tubule (Fig. 7B, e,f,h,i). In addition, *pou3f4* transcripts are detectable in groups of cells surrounding the eye (arrow head) (Fig. 7B, f,i) as well as in the condensing otic mesenchyme, which lies ventral to the otic vesicle (Fig. 7B, g). RT-qPCR analysis performed on different embryonic regions confirmed that *pou3f4* is strongly expressed in the head and the pronephric anlage (Fig. 7C).

Differential expression of *pou3f3* and *pou3f4* in the developing *X. laevis* pronephros

In order to define more precisely the expression domains of *pou3f3* and *pou3f4* in the developing *X. laevis* pronephros, we performed double staining by whole mount *in situ* hybridization. We compared *pou3f3* and *pou3f4* expression with that of *pax8*, which marks the entire presumptive pronephric region at the early and mid-tailbud stages (Carroll and Vize, 1996). The expression of *pou3f3* is restricted to the most anterior part of the pronephric anlage (Fig. 8A, d,e), whereas *pou3f4* is expressed in the entire pronephric anlage at the exception of the most dorso-anterior part (Fig. 8A, h,i). Transverse sections confirm these observations and reveal that *pou3f3* and *pou3f4* expression within the pronephric mesoderm is restricted to the somatic layer that gives rise to the pronephric tubule. No expression is detected in the splanchnic layer that will form the glomus (Fig. 8A, f,g,j,k). At the tadpole stage, the pronephric tubule is segmented along the proximo-distal axis into proximal, intermediate, distal, and connecting tubule (Raciti *et al.*, 2008). In contrast to *pax8*, neither

pou3f3 nor *pou3f4* is expressed in the proximal tubule (Fig. 8B). The *pou3f3* signal is in the intermediate tubule and the distal tubule, but expression in the latter declines as maturation of the tubule progresses (Fig. 8B, d-f) (Fig. 6B, f-i). The *pou3f4* gene is

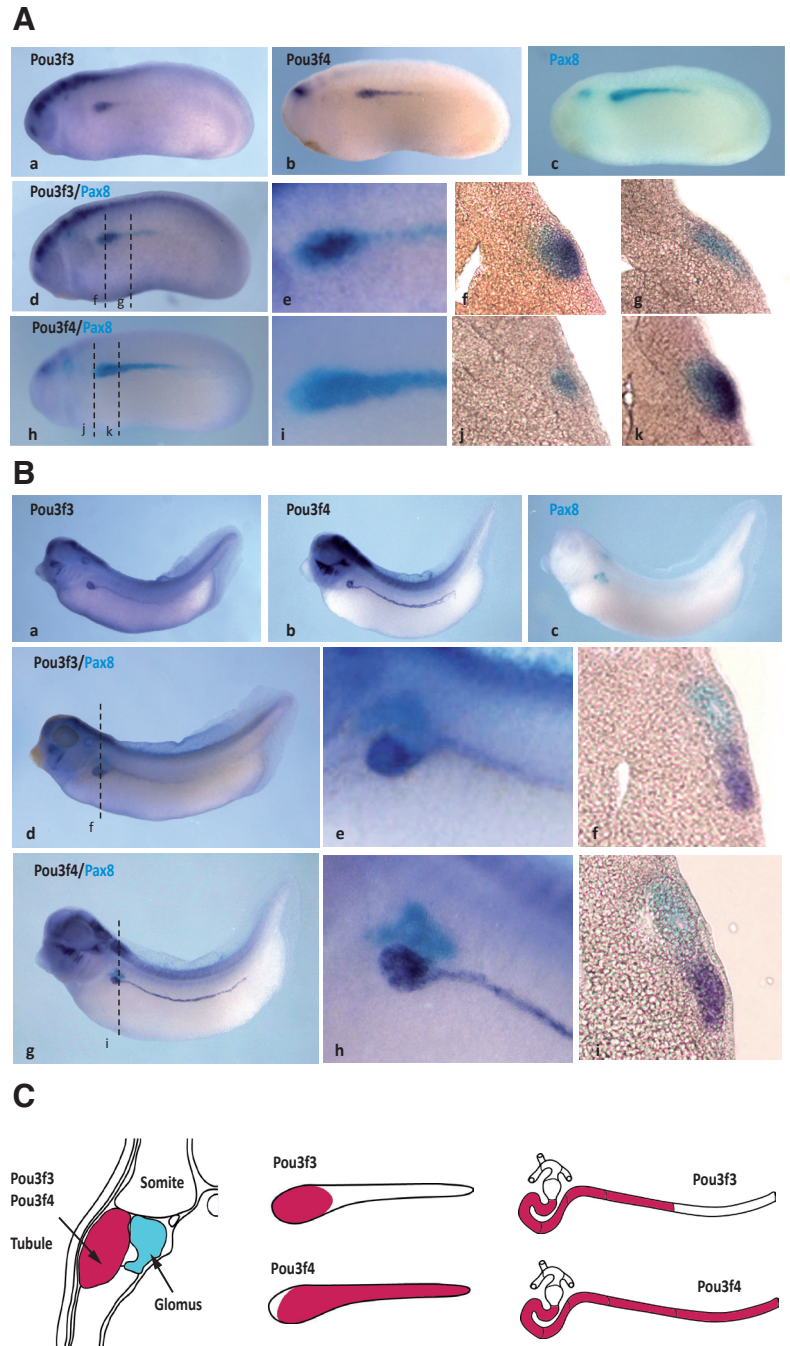


Fig. 8. Differential pronephric expression of *pou3f3* and *pou3f4* in *Xenopus laevis*. Whole mount *in situ* hybridization analysis of pronephric expression of *pou3f3* and *pou3f4* (dark blue) compared to *pax8* (light blue) in tailbud-stage embryos (stage 25) (A) and in the differentiated tubule in late tailbud-stage embryos (st 35) (B). Transverse sections in the anterior (A, f, j) and posterior part (A, g, k) of the anlage, and in the anterior part of the tubule (B, f, i). (C) Schematic representation of *pou3f3* and *pou3f4* expression in the pronephros: transverse section of a tailbud-stage embryo (left), lateral view of the pronephric anlage (middle) and of the differentiated tubule (right).

strongly expressed in the intermediate and distal tubule as well as the connecting tubule (Fig. 8B, g-i).

Discussion

The present study aims at characterizing the class 3 POU transcription factor complement of vertebrates, with a special focus on the *pou3f* genes from the frog *X. laevis*. Amino acid alignments revealed the general conservation of vertebrate Pou3f class proteins. Based on the fact that non-vertebrates generally encode only a single *pou3f* ortholog, the results of our phylogenetic and synteny analyses further indicate that the four vertebrate *pou3f* genes result from two successive duplications of a single ancestral *pou3f* gene in the last common ancestor of all vertebrates. The evolutionary history of the vertebrate *pou3f* class is thus consistent with the hypothesis that two whole-genome duplication (WGD) events occurred during early vertebrate evolution (Van de Peer et al., 2017). The existence of two *pou3f2* and *pou3f3* paralogs in teleost fish further supports the scenario of an additional, third, WGD marking the evolutionary diversification of the teleost fish lineage (Van de Peer et al., 2017). Intriguingly, we also found two examples of lineage-specific *pou3f* gene losses in teleost fish: *pou3f4* in the zebrafish and *pou3f2a* in the medaka. Future work will have to address, how widespread these lineage-specific *pou3f* gene losses are in teleost fish, whether they are directly linked to the third WGD and thus to the increased teleost fish *pou3f* complement, and whether they compensate, for example, gene dosage effects.

Our results show that all four *X. laevis pou3f* genes are expressed during neurulation in the forming neural tube and that their expression is maintained in the brain, mostly in the dorsal part, at tailbud stages. Neural expression of *Xenopus pou3f3* has already been described and our results largely confirm the published data (Square et al., 2015). Our results further highlight an evolutionary conserved expression of *pou3f* members in neural tissues. In mice, for example, *pou3f1* is expressed in the anterior neuro-ectoderm at E7.5 (Zhu et al., 2014). While the activity of this gene is subsequently required in the forebrain and midbrain for the regulation of neural commitment (Zhu et al., 2014), *pou3f4* is involved in neuron differentiation (Zhao, 2013). Furthermore, *pou3f2* and *pou3f3* show similar expression in the nervous system and a high level of functional redundancy. They are expressed in the neocortex, primarily in neurons of layers II-IV, and the analysis of *pou3f2/pou3f3* double mutants showed that both are involved in cortical neural migration, layer production, and neurogenesis (Cook and Sturm, 2008). Similarly, partial redundancy of *pou3f1* and *pou3f2* in Schwann cell differentiation has been described (Cook and Sturm, 2008). Interestingly, we showed that *pou3f1*, known to be involved in epidermal keratinocyte differentiation in mammals, is expressed in the *Xenopus* epidermis (Zhao, 2013). We also observed that *pou3f2*, *pou3f3*, and *pou3f4* are expressed in the developing *Xenopus* ear, as previously described in the mouse (Mutai et al., 2009, Phippard et al., 1999). Together with the fact that *pou3f4* is responsible for X-linked deafness type 3 in humans (Zhao, 2013), these data suggest a conserved role for *pou3f4* during vertebrate ear development. Of note, we did not find *pou3f4* expression in the mesoderm during gastrulation, contrary to what has previously been published (Witta et al., 1995). Our result has been confirmed by RT-qPCR on dissected gastrulae, with no significant expression having been detected in the mesoderm

compared to other tissues (Fig. S3). Given that the authors of the previous study used an *in situ* hybridization probe targeting the entire *pou3f4* sequence (Witta et al., 1995), this full-length probe might have also recognized other *pou3f* genes via the conserved POU-domain, for example *pou3f1*, which is highly expressed in the mesoderm during gastrulation.

Here, we show for the first time that *pou3f3* and *pou3f4*, but neither *pou3f1* nor *pou3f2*, are expressed in the developing *Xenopus* pronephros. In mice, *pou3f3* is expressed in the renal vesicle of the developing metanephros, and, later on, its expression is restricted to Henle's loop and to the distal convoluted tubule. The *pou3f3* gene has been shown to play a crucial role in the development of distinct nephron segments: *pou3f3* knock-out mice exhibit impaired elongation and differentiation of the developing Henle's loop and perinatal death due to renal failure (Nakai et al., 2003). More recently, analysis of the mouse mutant *Pou3f3^{L423P}*, characterized by a point mutation that leads to the alteration of a specific amino acid affecting the conserved homeobox domain of the protein, further revealed an involvement of *pou3f3* in the regulation of the overall number of developing nephrons (Rieger et al., 2016). Our results suggest a conserved role for *pou3f3* during vertebrate kidney development, as, in *Xenopus*, *pou3f3* is expressed in the anterior part of the pronephric anlage and later on in the intermediate and distal pronephric tubule, which is the structural and functional analog of Henle's loop (Raciti et al., 2008). We also observed that *pou3f4* is expressed in the developing *Xenopus* pronephros, but with a slightly different pattern than *pou3f3*. It is therefore interesting to note that part of the pronephric anlage and some tubule segments express both *pou3f3* and *pou3f4*, suggesting a possible redundancy or synergy, whereas some pronephric structures express only *pou3f3* (the most proximal part of the anlage) or *pou3f4* (the most distal part of the anlage and the tubule). In mice, three independent transcriptomic analyses have established that *pou3f4* is expressed in the ureteric bud, but not in the renal vesicle at E11.5 (Georgas et al., 2009, Schmidt et al., 2005, Smeeton et al., 2016), suggesting that *pou3f3* and *pou3f4* are also differentially expressed during metanephros development in mice. Together, these data suggest that *pou3f3* and *pou3f4* could have both distinct and redundant functions during kidney development in vertebrates. It will be important to perform single and double loss of function analyses in *Xenopus* to study the functional conservation of these genes during vertebrate kidney development.

Materials and Methods

Sequence alignments, phylogenetic tree calculations and genomic linkage analyses

Amino acid sequences included in the analysis were obtained by BLAST searches and are listed in Supplementary Table S1. Alignments were performed using MUSCLE as implemented in MEGA7 (Kumar et al., 2016) and then refined by eye. The final alignment included 42 amino acid sequences with a total of 317 positions (Fig. S1). Sequence identities for full-length *X. laevis* Pou3f proteins and their subdomains were calculated using a BioEdit sequence identity matrix (Hall, 1999). Phylogenetic trees were calculated with both the Maximum Likelihood (ML) and Bayesian inference (BI) methods, using a Dayhoff matrix-based substitution model with a discreet Gamma distribution (Schwarz and Dayhoff, 1979). ML tree calculations were conducted in MEGA7 (Kumar et al., 2016) with the robustness of each node being estimated by bootstrap analyses (in 1000 pseudoreplicates) (Felsenstein, 1985). BI trees were calculated using

MrBayes version 3.1.2 (Huelsenbeck and Ronquist, 2001) in 1,000,000 generations with sampling of trees every 100 generations and a burn-in period of 25%. The branching pattern of the ML tree was retained in the final tree figure, displaying, at each node, the bootstrap support of the ML analysis as well as the posterior probability support of the BI analysis. The tree is drawn to scale, with branch lengths indicating the number of substitutions per site. Synteny analyses were performed using Genomicus v89.02 (Louis *et al.*, 2015) and complemented manually based on genome locus searches of the NCBI database (Altschul *et al.*, 1990). The final synteny figure was adapted from the Genomicus output.

X. laevis embryos and dissections

X. laevis were purchased from the CNRS *Xenopus* breeding Center (Rennes, France). Embryos were obtained after artificial fertilization and were raised in modified Barth's solution (MBS). Staging was carried out according to the normal table of *X. laevis* development (Nieuwkoop, 1967). Dissections were performed as previously described (Le Bouffant *et al.*, 2014).

Real-time quantitative PCR

RNA extraction, reverse transcription, and real-time quantitative polymerase chain reaction (RT-qPCR) experiments were carried out as previously described (Le Bouffant *et al.*, 2014). The Comparative Ct method was used to determine the relative quantities of mRNA, using *ODC* mRNA as the endogenous reporter. Identical results were obtained using β -*actin* mRNA as the endogenous reporter (data not shown). Each RNA sample was analyzed in duplicates. All primers were used at a final concentration of 400 nM. Sequences of the oligonucleotides used are given in Supplementary Table S2. Each data point represents the mean \pm standard error of the mean (SEM) of at least three independent experiments. Data were analyzed using R Commander (R software) by paired Student's t-test.

In situ hybridization

Whole mount *in situ* hybridizations were carried out as previously reported (Le Bouffant *et al.*, 2014). To obtain the plasmids for synthesis of antisense RNA probes, PCR products were generated from cDNA libraries using specific primers listed in Supplementary Table S3. PCR products were cloned into the pCRII vector according to manufacturer's instructions (Invitrogen), and digoxigenin-labeled antisense RNA probes were transcribed from linearized plasmids using SP6 or T7 polymerase. After *in situ* hybridization, embryos were sectioned at 60 μ m thickness using a vibratome. *In situ* hybridization with a sense probe was performed as a control for each antisense probe. Signal above background was never detected with the sense probes.

Acknowledgements

We want to thank Sylvie Authier, Edouard Manzoni, and Abdelkrim Manioui for excellent technical assistance in the maintenance of the *Xenopus* animal facility, Aurellia Galliot for help with *in situ* hybridization, and Sophie Gournet for illustration work. The authors are further indebted to Philippe Dru and João E. Carvalho for supporting the bioinformatic analyses. This work was supported by grants from the CNRS and from Sorbonne Université. CCE was financed by a 2014-2017 "Contrat Doctoral" from the doctoral school "Complexité du Vivant".

References

ALTSCHUL, S.F., GISH, W., MILLER, W., MYERS, E.W. and LIPMAN, D.J. (1990). Basic local alignment search tool. *J Mol Biol* 215: 403-410.

CARROLL, T.J. and VIZE, P.D. (1996). Wilms' tumor suppressor gene is involved in the development of disparate kidney forms: evidence from expression in the *Xenopus* pronephros. *Dev Dyn* 206: 131-138.

COOK, A.L. and STURM, R.A. (2008). POU domain transcription factors: BRN2 as a regulator of melanocytic growth and tumorigenesis. *Pigment Cell Melanoma*

Res 21: 611-626.

FELSENSTEIN, J. (1985). Confidence limits on phylogenies: an approach using the bootstrap. *Evolution* 39: 783-791.

GEORGAS, K., RUMBALLE, B., VALERIUS, M.T., CHIU, H.S., THIAGARAJAN, R.D., LESIEUR, E., ARONOW, B.J., BRUNSKILL, E.W., COMBES, A.N., TANG, D. *et al.*, (2009). Analysis of early nephron patterning reveals a role for distal RV proliferation in fusion to the ureteric tip via a cap mesenchyme-derived connecting segment. *Dev Biol* 332: 273-286.

HALL, T.A. (1999). BioEdit: a user-friendly biological sequence alignment editor and analysis program for Windows 95/98/NT. *Nucl Acids Symp Ser* 41: 95-98.

HUELSENBECK, J.P. and RONQUIST, F. (2001). MrBayes: Bayesian inference of phylogeny. *Bioinformatics* 17: 754-755.

KUMAR, S., STECHER, G. and TAMURA, K. (2016). MEGA7: Molecular Evolutionary Genetics Analysis version 7.0 for bigger datasets. *Mol Biol Evol* 33: 1870-1874.

LE BOUFFANT, R., CUNIN, A.C., BUISSON, I., CARTRY, J., RIOU, J.F. and UMBHAUER, M. (2014). Differential expression of *arid5b* isoforms in *Xenopus laevis* pronephros. *Int J Dev Biol* 58: 363-368.

LOUIS, A., NGUYEN, N.T., MUFFATO, M. and CROLLIUS, H.R. (2015). Genomicus update 2015: KaryoView and MatrixView provide a genome-wide perspective to multispecies comparative genomics. *Nucleic Acids Res* 43: D682-689.

MUTAI, H., NAGASHIMA, R., SUGITANI, Y., NODA, T., FUJII, M. and MATSUNAGA, T. (2009). Expression of *Pou3f3/Brn-1* and its genomic methylation in developing auditory epithelium. *Dev Neurobiol* 69: 913-930.

NAKAI, S., SUGITANI, Y., SATO, H., ITO, S., MIURA, Y., OGAWA, M., NISHI, M., JISHAGE, K., MINOWA, O. and NODA, T. (2003). Crucial roles of Brn1 in distal tubule formation and function in mouse kidney. *Development* 130: 4751-4759.

NIEUWKOOP, P.D.A.F., J. (1967). *Normal table of Xenopus laevis (Daudin)*. North-Holland Publishing Company. Amsterdam.

PHIPPARD, D., LU, L., LEE, D., SAUNDERS, J.C. and CRENSHAW, E.B., 3RD. (1999). Targeted mutagenesis of the POU-domain gene *Brn4/Pou3f4* causes developmental defects in the inner ear. *J Neurosci* 19: 5980-5989.

RACITI, D., REGGIANI, L., GEFFERS, L., JIANG, Q., BACCCHION, F., SUBRIZI, A.E., CLEMENTS, D., TINDAL, C., DAVIDSON, D.R., KAISLING, B. *et al.*, (2008). Organization of the pronephric kidney revealed by large-scale gene expression mapping. *Genome Biol* 9: R84.

RIEGER, A., KEMTER, E., KUMAR, S., POPPER, B., AIGNER, B., WOLF, E., WANKE, R. and BLUTKE, A. (2016). Missense mutation of POU domain class 3 transcription factor 3 in *Pou3f3^{423P}* mice causes reduced nephron number and impaired development of the thick ascending limb of the loop of Henle. *PLoS One* 11: e0158977.

RYAN, A.K. and ROSENFELD, M.G. (1997). POU domain family values: flexibility, partnerships, and developmental codes. *Genes Dev* 11: 1207-1225.

SCHMIDT, A., SOMMER, F., REINER, M., KLOTZ, T., ENGELMANN, U., ADDICKS, K. and BLOCH, W. (2005). Differential endostatin binding to bladder, prostate and kidney tumour vessels. *BJU Int* 95: 174-179.

SCHWARZ R. and DAYHOFF M. (1979). Matrices for detecting distant relationships. In *Atlas of protein sequences* (Ed. M. Dayhoff). National Biomedical Research Foundation, Washington D.C., pp. 353-358.

SMEETON, J., DHIR, P., HU, D., FEENEY, M.M., CHEN, L. and ROSENBLUM, N.D. (2016). Integrin-linked kinase controls renal branching morphogenesis via dual specificity phosphatase 8. *J Am Soc Nephrol* 27: 1465-1477.

SQUARE, T., JANDZIK, D., CATTELL, M., COE, A., DOHERTY, J. and MEDEIROS, D.M. (2015). A gene expression map of the larval *Xenopus laevis* head reveals developmental changes underlying the evolution of new skeletal elements. *Dev Biol* 397: 293-304.

VAN DE PEER, Y., MIZRACHI, E. and MARCHAL, K. (2017). The evolutionary significance of polyploidy. *Nat Rev Genet* 18: 411-424.

WITTA, S.E., AGARWAL, V.R. and SATO, S.M. (1995). *XIPOU 2*, a noggin-inducible gene, has direct neuralizing activity. *Development* 121: 721-730.

ZHAO, F.Q. (2013). Octamer-binding transcription factors: genomics and functions. *Front Biosci* 18: 1051-1071.

ZHU, Q., SONG, L., PENG, G., SUN, N., CHEN, J., ZHANG, T., SHENG, N., TANG, W., QIAN, C., QIAO, Y. *et al.*, (2014). The transcription factor Pou3f1 promotes neural fate commitment via activation of neural lineage genes and inhibition of external signaling pathways. *eLife* 3: e02224.

Further Related Reading, published previously in the *Int. J. Dev. Biol.*

Chromatin assembly and transcriptional cross-talk in *Xenopus laevis* oocyte and egg extracts

Wei-Lin Wang and David Shechter
Int. J. Dev. Biol. (2016) 60: 315-320
<https://doi.org/10.1387/ijdb.160161ds>

Expressional characterization of mRNA (guanine-7) methyltransferase (rnmt) during early development of *Xenopus laevis*

Ashwin Lokapally, Sanjeeva Metikala and Thomas Hollemann
Int. J. Dev. Biol. (2016) 60: 65-69
<https://doi.org/10.1387/ijdb.150409th>

pdzrn3 is required for pronephros morphogenesis in *Xenopus laevis*

Silvia Marracci, Alberto Vangelisti, Vittoria Raffa, Massimiliano Andreazzoli and Luciana Dente
Int. J. Dev. Biol. (2016) 60: 57-63
<https://doi.org/10.1387/ijdb.150381ld>

Expression of the novel gene *Ened* during mouse and *Xenopus* embryonic development

Renata Meszaros, Ina Strate, Edgar M. Pera and Madeleine Durbeej
Int. J. Dev. Biol. (2008) 52: 1119-1122
<https://doi.org/10.1387/ijdb.082700rm>

The role of XTRAP-gamma in *Xenopus* pronephros development

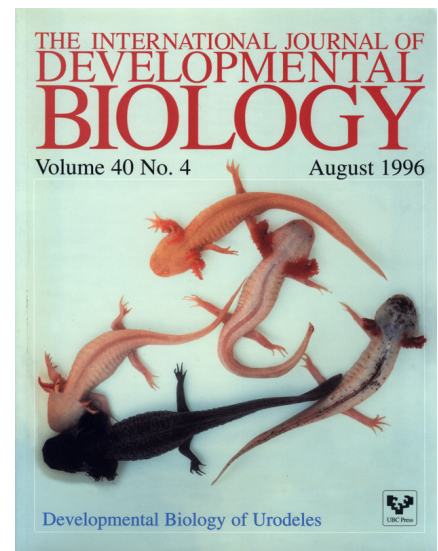
Dong-hui Li, Techuan Chan, Reiko Satow, Shinji Komazaki, Kouhei Hashizume and Makoto Asashima
Int. J. Dev. Biol. (2005) 49: 401-408
<http://www.intjdevbiol.com/web/paper/052005dl>

Embryonic expression of *Xenopus* SGLT-1L, a novel member of the solute carrier family 5 (SLC5), is confined to tubules of the pronephric kidney

Samer R Eid, Anne Terrettaz, Katsumi Nagata and André W Brändli
Int. J. Dev. Biol. (2002) 46: 177-184
<http://www.intjdevbiol.com/web/paper/11902681>

Towards a molecular anatomy of the *Xenopus* pronephric kidney

A W Brändli
Int. J. Dev. Biol. (1999) 43: 381-395
<http://www.intjdevbiol.com/web/paper/10535314>



5 yr ISI Impact Factor (2016) = 2.421

